

# On the Relation between Random Walks and Quantum Walks

Stefan Boettcher<sup>1</sup>, Stefan Falkner<sup>1</sup>, and Renato Portugal<sup>2</sup>

<sup>1</sup>Department of Physics, Emory University, Atlanta, GA 30322; USA

<sup>2</sup>Laboratório Nacional de Computação Científica, Petrópolis, RJ 25651-075; Brazil

We propose a general relation between the walk dimensions  $d_w$  of random walks and quantum walks, which illuminates fundamental aspects of the walk dynamics, such as its mean-square displacement. To this end, we extend the renormalization group analysis (RG) of the stochastic master equation to one with a unitary propagator. As in the classical case, the solution  $\rho(x, t)$  in space and time of this quantum walk equation exhibits a scaling collapse for the variable  $x^{d_w}/t$ . In all cases studied, we find that  $d_w$  of the discrete-time quantum walk with the Grover coin takes on exactly half the value found for the random walk on the same geometry, irrespective of whether it is a homogeneous lattice or a heterogeneous network. We demonstrate this circumstance for several networks with distinct properties using exact RG and confirm the collapse in each case with extensive numerical simulation.

Like random walks, quantum walks are rapidly gaining a central role in describing a considerable range of phenomena, from experiments in quantum transport [1–4] to universal models of quantum computing [5, 6]. Quantum walks are the “engine” that drives quantum search algorithms [7], with the prospect of a quadratic speed-up over classical search algorithms. Yet, despite considerable efforts, our understanding of quantum walks still lacks behind that of random walks [8–11], as they exhibit a much broader spectrum of behaviors awaiting categorization and context, even for simple lattices [12–20].

In this Letter, we propose a relation bridging between random and quantum walks that elucidates their scaling properties at long times and distances on arbitrary networks, which is intimately linked to the dynamics of their spread as well as their algorithmic performance [21, 22]. We find that the walk dimension  $d_w$  for a discrete-time quantum walk with a Grover coin is half of that for the corresponding random walk,

$$d_w^{QW} = \frac{1}{2} d_w^{RW}. \quad (1)$$

This relation appears to be rather general, and we show that it holds even if the walks are anomalous and the geometry lacks translational symmetry.

The probability density  $\rho(\vec{x}, t)$  to detect a walk at time  $t$  at site  $\vec{x}$ , a distance  $x$  from its origin, for random walks obeys the scaling collapse [9],

$$\rho(\vec{x}, t) \sim t^{-\frac{d_f}{d_w}} f\left(x/t^{\frac{1}{d_w}}\right). \quad (2)$$

where  $d_f$  is the (possibly fractal) dimension of the network. On a translationally invariant lattice in any spatial dimension  $d (= d_f)$ , it is easy to show that the walk is always purely “diffusive”,  $d_w = 2$ , with a Gaussian scaling function  $f$ . The scaling in Eq. (2) still holds when translational invariance is broken in certain ways or the network is fractal (i.e.,  $d_f$  is non-integer). However, anomalous diffusion with  $d_w \neq 2$  may arise in many transport processes [9, 23].

For quantum walks, the only known value for a finite walk dimension is that for ordinary lattices [24], where Eq. (2) generically holds with  $d_w = 1$ , indicating a “ballistic” spreading of the quantum walk from its origin. This ability to explore a given geometry that much faster than diffusion is essential for the effectiveness of quantum search algorithms [21, 22]. While this value satisfies Eq. (1), it does little to justify it. In fact, the simplicity and robustness of the value of  $d_w$  is surprising, even on a simple line,  $d = 1$ . We can picture  $\rho(\vec{x}, t)$  as resulting from the superposition of all paths that lead from the origin  $\vec{x}_0 = 0$  to site  $\vec{x}$  in  $t$  steps, weighted by the probability of each path. Classically, each path merely receives a factor  $\frac{1}{2}$  for the probability to branch left or right at every step (in the simplest case). Then, all paths have the *same* weight  $2^{-t}$  and  $\rho(\vec{x}, t)$  becomes distinguished only by the *number* of path that can reach  $\vec{x}$ , with its variance after  $t$  steps,  $\langle \vec{x}^2 \rangle \sim t$ , providing  $d_w = 2$ . For the widely used description of a discrete-time quantum walk [13],  $\rho(\vec{x}, t)$  becomes the modulo-squared of the weighted sum over the very same paths. At any branch, each path receives a *different* complex factor to its weight. It is then the subtle superposition of these complex weights, and their interference in the square-modulus, that determines the spread of  $\rho(\vec{x}, t)$ . Although quantum walks may possess extra internal degrees of freedom, asymptotically they invariably result in  $d_w = 1$ .

The distinct manner in which random walk and quantum walk attain their respective probability densities  $\rho(\vec{x}, t)$  suggests that a relation between their walk dimension,  $d_w^{RW}$  and  $d_w^{QW}$ , should be purely accidental. Any relation would be limited to a few geometries with special constraints on quantum interference effects, such as those imposed by translational invariance. Nevertheless, based on a number of diverse *fractal* networks for which we have calculated non-trivial values of  $d_w$  for a widely used description of quantum walks, we find the succinct relation in Eq. (1) without exception satisfied. This suggests that the common geometry leaves a deeper imprint on the long-time behavior of both, random and quantum walks,

Table I. Fractal and walk dimensions for the networks considered here. The classical values for  $d_f$  and  $d_w^{RW}$  are known for DSG [9] and HN3 [26], or derived here for MK. The values for  $d_w^{QW}$  are determined with the RG. Each case satisfies Eq. (1).

Network	$d_f$	$d_w^{RW}$	$d_w^{QW}$
MK3	$\log_4(7)$	$\log_4(21) \approx 2.196$	$1.098079\dots$
MK4	$\log_4(13)$	$\log_4\left(\frac{247}{7}\right) \approx 2.571$	$1.285253\dots$
DSG	$\log_2(3)$	$\log_2(5) \approx 2.322$	$1.160964\dots$
HN3	2	$\log_2(24 - 8\sqrt{5}) \approx 2.612$	$1.305758\dots$

than might have been expected from their rather distinct dynamics. Such insight is likely to make quantum walk based algorithms more predictable for networks [25].

The dynamics for a discrete-time walk with a coin, classical or quantum, is determined by the master-equation,

$$|\Psi_{t+1}\rangle = \mathcal{U}|\Psi_t\rangle. \quad (3)$$

In the site-basis  $|\vec{x}\rangle$  of any network, we can describe the state of the system in terms of the site amplitudes  $\psi_{\vec{x},t} = \langle \vec{x}|\Psi_t\rangle$ . For a classical random walk, the probability density in Eq. (2) is simply given by the site amplitude itself,  $\rho(\vec{x},t) = \psi_{\vec{x},t}$ , while for the quantum walk it is  $\rho(\vec{x},t) = |\psi_{\vec{x},t}|^2$ . Accordingly, the propagator  $\mathcal{U}$  is a stochastic Bernoulli coin for a random walk, while it must be *unitary* for a quantum walk, usually composed as

$$\mathcal{U} = \mathcal{S}(\mathbb{1} \otimes \mathcal{C}), \quad (4)$$

with coin  $\mathcal{C}$  and shift  $\mathcal{S}$ . Unitarity,  $\mathcal{U}^\dagger \mathcal{U} = \mathbb{1}$ , demands [27, 28] that the coin is a unitary matrix of rank  $r > 1$ , such that the site amplitudes  $\psi_{\vec{x},t}$  become complex  $r$ -dimensional vectors in “coin”-space. For simplicity, this quantum walk is commonly studied on networks of regular degree  $r$  for all  $\vec{x}$ , so that the same coin can be applied at every site. Every step consists of a “coin flip”, the multiplication of  $\psi_{\vec{x},t}$  with  $\mathcal{C}$ , followed by the shift  $\mathcal{S}$  that transfers each component of  $\mathcal{C} \cdot \psi_{\vec{x},t}$  to exactly one of the  $r$  neighbors of  $\vec{x}$ .

To test Eq. (1) for nontrivial values for  $d_w$ , we study the quantum walk on four fractal networks of degrees  $r = 3$  and 4, with the widely used Grover coin [7, 20], i.e., the  $r \times r$  matrix

$$\mathcal{C}_G^{(r)} = \frac{2}{r} \begin{pmatrix} 1 - \frac{r}{2} & 1 & \dots & 1 \\ 1 & \ddots & & \vdots \\ \vdots & & \ddots & 1 \\ 1 & \dots & 1 & 1 - \frac{r}{2} \end{pmatrix}. \quad (5)$$

Namely, we study two Migdal-Kadanoff networks [29, 30] (MK3 and MK4), the dual Sierpinski gasket [9, 11] (DSG), and the Hanoi network [26] (HN3). These networks lack translational invariance, but exhibit self-similarity instead. DSG more closely resembles a  $2d$  lattice, MK networks have a hierarchical structure, while

HN3 is a hyperbolic [31] small-world network. For each network, the anomalous classical result for  $d_w$  of the random walk and their fractal dimension  $d_f$  are easily obtained via the renormalization group (RG) method [11, 30, 32], described below for MK3; the RG for MK4, DSG and HN3 is discussed in the Appendix. By extending RG to quantum walks [33], we obtain the first exact scaling exponents for quantum walks on heterogeneous structures. All results are summarized in Table I.

The fractal dimension [9, 11] is defined via the scaling  $N \sim L^{d_f}$ , where  $N$  stands for the number of sites that are at most  $L$  hops away from a given site. For MK3, as shown in Fig. 1, the number of edges (and, hence, sites) changes 7-fold between iterations while distances between two sites changes 4-fold, implying  $d_f = \log_4(7)$ .

To calculate the walk dimension with RG, we first apply the Laplace transform [10, 11, 32],

$$|\tilde{\Psi}(z)\rangle = \sum_{t=0}^{\infty} z^t |\Psi_t\rangle, \quad (6)$$

to Eq. (3), providing algebraic equations with generalized hopping operators that now depend on  $z$ . For instance, after any number of iterations, MK3 entirely consist of graphlets, as depicted in the top panel of Fig. 1. For sites  $3, \dots, 6$ , it represents the *linear* system of equations [34]

$$\begin{pmatrix} \tilde{\psi}_3 \\ \tilde{\psi}_4 \\ \tilde{\psi}_5 \\ \tilde{\psi}_6 \end{pmatrix} = \begin{bmatrix} A & 0 & M & B & C & 0 \\ 0 & 0 & B & M & A & C \\ 0 & 0 & C & A & M & B \\ 0 & A & 0 & C & B & M \end{bmatrix} \cdot \begin{pmatrix} \tilde{\psi}_1 \\ \tilde{\psi}_2 \\ \tilde{\psi}_3 \\ \tilde{\psi}_4 \\ \tilde{\psi}_5 \\ \tilde{\psi}_6 \end{pmatrix} \quad (7)$$

with hopping operators  $A, B, C$ , and  $M$ , where  $M$  allows for self-interaction at each site. (In the original graph  $M = 0$ .) Taking advantage of self-similarity, we express one iteration of the network in terms of the next smaller one but with “renormalized” values for the hopping operators. To that end, we solve for  $\tilde{\psi}_3, \dots, \tilde{\psi}_6$  in term of  $\tilde{\psi}_1$  and  $\tilde{\psi}_2$  and insert into the equations for the remaining site amplitudes, such that

$$\tilde{\psi}_{1,2} = M\tilde{\psi}_{1,2} + A\tilde{\psi}_{3,6} + B\tilde{\psi}_{\overline{3},\overline{6}} + C\tilde{\psi}_{\overline{\overline{3}},\overline{\overline{6}}}, \quad (8)$$

$$= M'\tilde{\psi}_{1,2} + A'\tilde{\psi}_{2,1} + B'\tilde{\psi}_{\overline{2},\overline{1}} + C'\tilde{\psi}_{\overline{\overline{2}},\overline{\overline{1}}}, \quad (9)$$

where primes indicate the renormalized hopping operators as depicted in the bottom panel of Fig. 1. Repetition then relates the  $k+1$  (primed) iterate to the  $k$ -th (unprimed) iterate, yielding the (highly non-linear) RG-flow [30, 32],

$$(A_{k+1}, B_{k+1}, C_{k+1}, M_{k+1}) = \mathcal{RG}(A_k, B_k, C_k, M_k), \quad (10)$$

that characterizes the effective dynamics between domains of sites of width  $L_k$  and  $L_{k+1}$  by renormalized hopping operators.

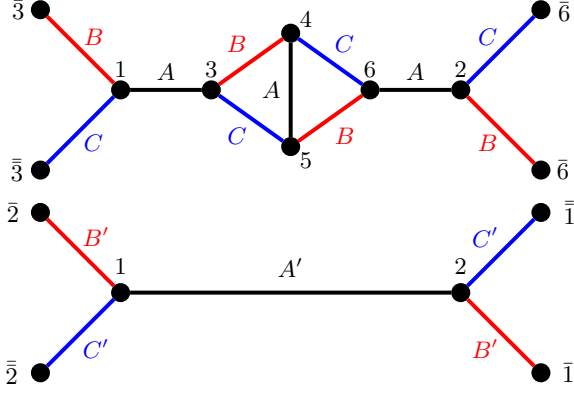


Figure 1. Iterative scheme for the decimation of the Migdal-Kadanoff network MK3. Interior sites  $3, \dots, 6$  in the graph-let (top) are algebraically eliminated, see Eq. (7), and replaced by a single edge (bottom) with an effective (“renormalized”) hopping operator  $A'$  by which the terminal site amplitudes 1, 2 on either end of the edge shift their components between each other. (Edges from sites 1, 2 to sites in equivalent neighboring structures are indicated by overbars.) While renormalization is shown for an edge of type  $A$  only, types  $B$  and  $C$  obtain via cyclic permutation  $A \rightarrow B \rightarrow C \rightarrow A$ . Constructing MK3 for simulations proceeds by replacing every edge (bottom) by the corresponding graph-let (top) recursively for  $k$  iterations, as discussed in the Appendix.

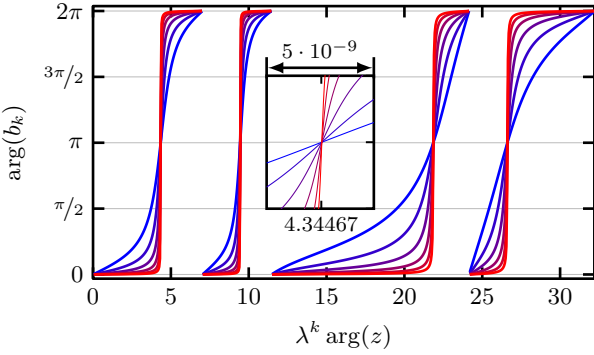


Figure 2. Scaling collapse of the phase of  $b_k$  in Eq. (12) near the fixed point  $z = 1$  with  $\lambda = \sqrt{21}$ . The inset shows the region around the first intersection. In the main panel,  $k = 4, 6, \dots, 14$  while  $k = 50, 52, \dots, 60$  for the inset, corresponding to a system size of MK3 with up to  $N \approx 7^{60} \approx 10^{51}$  sites.

In case of the unbiased random walk, all the hopping operators become simple scalars,  $A = B = C = a$ , and setting  $M = 1 - b$ , Eq. (10) provides

$$\begin{aligned} a_{k+1} &= \frac{2a_k^4}{b_k^3 - 4a_k^2b_k - a_kb_k^2}, \\ b_{k+1} &= b_k + \frac{3a_k^2(2a_k - b_k)(a_k + b_k)}{b_k^3 - 4a_k^2b_k - a_kb_k^2}, \end{aligned} \quad (11)$$

with the initial conditions  $a_0 = z/3$  and  $b_0 = 1$ . For  $z \rightarrow 1$ , the relevant fixed point (describing the infinite system,  $k \rightarrow \infty$ ) is  $a_\infty, b_\infty \rightarrow 0$ , i.e., domain width  $L_k \sim 4^k$

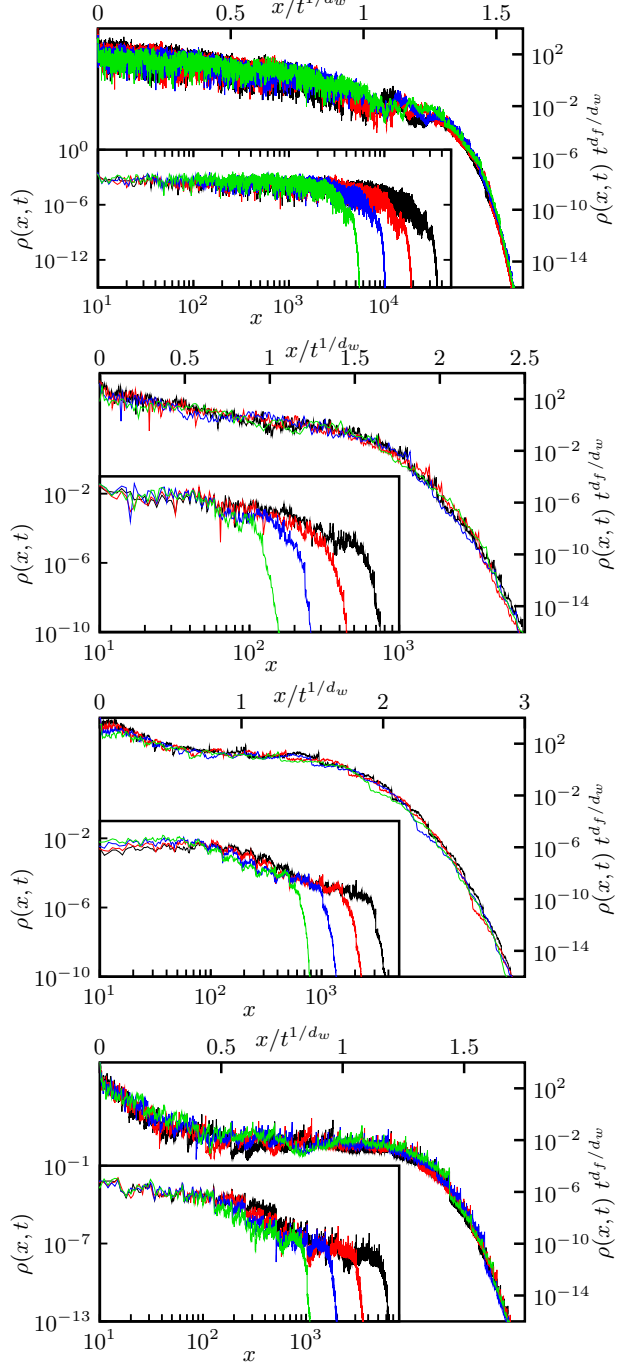


Figure 3. Data collapse of the probability density  $\rho(|\vec{x}|, t)$  according to Eq. (2) with  $d_f$  and  $d_w$  given in Tab. I. The data is obtained by direct simulations of quantum walks on the four different networks in this study. The inset of each panel shows the raw data. The top panel concerns MK3 with  $N = 2 \cdot 7^8 \approx 10^7$  sites at times  $t = 2^j$ ,  $j = 13, \dots, 16$ , from left to right in the inset. In the main panel, the data is collapse with  $d_f = \log_4(7)$  and  $d_w^{QW} = \log_4(21)/2$ . The 2<sup>nd</sup> panel concerns MK4 with  $N = 2 \cdot 13^5 \approx 7 \cdot 10^5$  sites at  $t = 2^j$ ,  $j = 10, \dots, 13$ , collapsed with  $d_f = \log_4(13)$  and  $d_w^{QW} = \log_{16}(247/7)$ . The 3<sup>rd</sup> panel concerns HN3 with  $N = 2^{24} \approx 1.7 \cdot 10^7$  sites at  $t = 2^j$ ,  $j = 11, \dots, 14$ , collapsed with  $d_f = 2$  and  $d_w^{QW} = \log_4(24 - 8\sqrt{5})$ . The 4<sup>th</sup> panel on the bottom concerns DSG with  $N = 3^{15} \approx 1.4 \cdot 10^7$  sites at  $t = 2^j$ ,  $j = 11, \dots, 14$ , collapsed with  $d_f = \log_2(3)$  and  $d_w^{QW} = \log_2(5)/2$ .

grow faster than the diffusive transport between them, as represented by  $a_k$ . With the scaling Ansatz  $a_k = 3^{-k}\alpha_k$  and  $b_k = 3^{-k}\beta_k$ , we resolve this boundary layer to find the fixed point  $\beta_\infty = 3\alpha_\infty$  with Jacobian eigenvalue  $\lambda = 21$  that relates to the rescaling of time,  $T_{k+1} = \lambda T_k$ , by the Tauberian theorems [10, 11, 32]. Then,  $L_{k+1} = 4L_k$  and  $T_k \sim L_k^{d_w}$  from Eq. (2), finally yield  $d_w^{RW} = \log_4(21)$ .

For the quantum walk, the hopping operators now

$$\begin{aligned} a_{k+1} &= \frac{-9a_k + 5a_k^3 + 9b_k + 3a_k b_k - 17a_k^2 b_k - 3a_k^3 b_k + 3b_k^2 + 14a_k b_k^2 - 3a_k^2 b_k^2 - 18a_k^3 b_k^2}{-18 - 3a_k + 14a_k^2 + 3a_k^3 - 3b_k - 17a_k b_k + 3a_k^2 b_k + 9a_k^3 b_k + 5b_k^2 - 9a_k^2 b_k^2}, \\ b_{k+1} &= \frac{-3a_k - a_k^2 + 3b_k + 4a_k b_k - 3a_k^2 b_k - b_k^2 + 3a_k b_k^2 + 6a_k^2 b_k^2}{6 + 3a_k - a_k^2 - 3b_k + 4a_k b_k + 3a_k^2 b_k - b_k^2 - 3a_k b_k^2}, \end{aligned} \quad (12)$$

with  $a_0 = b_0 = z$ . It can be shown that  $|a_k| = |b_k| \equiv 1$  for all  $k$ , reducing the RG parameters to just two real phases for  $a_k, b_k$ .

As explained in Ref. 33, the classical fixed-point analysis from above fails for the quantum walk. Unitary demands that information about  $\rho(\vec{x}, t)$  has to be recovered from an integral involving  $\tilde{\psi}_{\vec{x}}[a_k(z), b_k(z)]$  around the unit circle in the complex- $z$  plane. It is the *scaling collapse* of  $\{a, b\}_k(z) \sim f_{\{a, b\}}(\lambda^k \arg z)$ , and consequently any observable function of  $\tilde{\psi}_{\vec{x}}$ , over a finite support that allows to approximate  $d_w$  recursively with arbitrary accuracy. An illustration of the collapse for, say, the phase of  $b_k$  is shown in Fig. 2. Equivalent plots can be found in the Appendix for MK4, HN3, and DSG.

To justify these RG predictions for  $d_w$ , we resort to direct simulation of quantum walks to test Eq. (2). Those simulations cannot reach as extreme a system sizes as RG, but the collapse of the probability density  $\rho(x, t)$  over the entire network illustrates the consistency with the RG predictions, as shown in Fig. 3 for all four networks considered here.

This exact RG may be limited to specific networks, however, our present study demonstrates that RG can deliver unprecedented insights into the dynamics of quantum processes with a generality that transcend those limitation. The *universality* of these results, a central concern of RG [30], remains largely unexplored for quantum walks [33]. It is straightforward to show that, asymptotically, random walks on these networks are independent of the specific choices for a Bernoulli coin. However, for quantum walks, the most general unitary coin matrix  $\mathcal{C}$  for  $r = 3$  would already contain six free parameters that could impact the dynamics in unforeseen ways.

are matrices in coin-space, and the algebra gets more involved. Iterating the matrix-valued RG-flow in Eq. (10) numerically suggests that all matrices can be parametrized with merely two scalars, most conveniently in the form  $\{A, B, C\} = \frac{a+b}{2} (P_{\{1,2,3\}} \cdot \mathcal{C}_G)$  and  $M = \frac{a-b}{2} (\mathbf{1} \cdot \mathcal{C}_G)$ , where the  $3 \times 3$ -matrices  $[P_\nu]_{i,j} = \delta_{i,\nu} \delta_{\nu,j}$  (with  $\sum_{\nu=1}^3 P_\nu = \mathbf{1}$ ) facilitate the shift of the  $\nu$ -th component to a neighboring site. The RG-flow closes for

## ACKNOWLEDGEMENTS

SB and SF acknowledge financial support from the U. S. National Science Foundation through grant DMR-1207431. SB acknowledges financial support from CNPq through the “Ciéncia sem Fronteiras” program and thanks LNCC for its hospitality.

- [1] H. B. Perets, Y. Lahini, F. Pozzi, M. Sorel, R. Morandotti, and Y. Silberberg, Phys. Rev. Lett. **100**, 170506 (2008).
- [2] C. Weitenberg, M. Endres, J. F. Sherson, M. Cheneau, P. Schauss, T. Fukuhara, I. Bloch, and S. Kuhr, Nature **471**, 319 (2011).
- [3] L. Sansoni, F. Sciarrino, G. Vallone, P. Mataloni, A. Crespi, R. Ramponi, and R. Osellame, Phys. Rev. Lett. **108**, 010502 (2012).
- [4] A. Crespi, R. Osellame, R. Ramponi, V. Giovannetti, R. Fazio, L. Sansoni, F. D. Nicola, F. Sciarrino, and P. Mataloni, Nature Photonics **7**, 322 (2013).
- [5] A. M. Childs, Phys. Rev. Lett. **102**, 180501 (2009).
- [6] A. M. Childs, D. Gosset, and S. Webb, Science **339**, 791 (2013).
- [7] L. K. Grover, Phys. Rev. Lett. **79**, 325 (1997).
- [8] M. F. Shlesinger and B. J. West, eds., *Random walks and their applications in the physical and biological sciences* (American Institute of Physics, New York, 1984).
- [9] S. Havlin and D. Ben-Avraham, Adv. Phys. **36**, 695 (1987).
- [10] G. H. Weiss, *Aspects and Applications of the Random Walk* (North-Holland, Amsterdam, 1994).
- [11] B. D. Hughes, *Random Walks and Random Environments* (Oxford University Press, Oxford, 1996).
- [12] D. Aharonov, A. Ambainis, J. Kempe, and U. Vazirani, in *Proc. 33rd Annual ACM Symp. on Theory of Computing (STOC 2001)* (ACM, New York, NY, 2001) pp. 50–59.
- [13] A. Ambainis, E. Bach, A. Nayak, A. Vishwanath, and J. Watrous, in *Proceedings of the thirty-third annual*

ACM symposium on Theory of computing, STOC '01 (ACM, New York, NY, USA, 2001) pp. 37–49.

[14] E. Bach, S. Coppersmith, M. P. Goldschen, R. Joynt, and J. Watrous, *Journal of Computer and System Sciences* **69**, 562 (2004).

[15] A. M. Childs, E. Farhi, and S. Gutmann, *Quantum Information Processing*, *Quantum Information Processing* **1**, 35 (2002).

[16] A. M. Childs and J. Goldstone, *Phys. Rev. A* **70**, 022314 (2004).

[17] N. Konno, in *Quantum Potential Theory*, Lecture Notes in Mathematics, Vol. 1954, edited by U. Franz and M. Schürmann (Springer-Verlag: Heidelberg, Germany, 2008) pp. 309–452.

[18] F. Magniez, A. Nayak, P. C. Richter, and M. Santha, in *Proceedings of the twentieth Annual ACM-SIAM Symposium on Discrete Algorithms*, SODA '09 (Society for Industrial and Applied Mathematics, Philadelphia, PA, USA, 2009) pp. 86–95.

[19] E. Venegas-Andraca, *Quantum Information Processing* **11**, 1015 (2012).

[20] R. Portugal, *Quantum Walks and Search Algorithms* (Springer, Berlin, 2013).

[21] A. Ambainis, *SIAM J. Comput.* **37**, 210 (2007).

[22] A. M. Childs, R. Cleve, E. Deotto, E. Farhi, S. Gutmann, and D. A. Spielman, in *Proceedings of the Thirty-fifth Annual ACM Symposium on Theory of Computing*, STOC '03 (ACM, New York, NY, USA, 2003) pp. 59–68.

[23] J.-P. Bouchaud and A. Georges, *Physics Reports* **195**, 127 (1990).

[24] G. Grimmett, S. Janson, and P. F. Scudo, *Physical Review E* **69**, 026119+ (2004).

[25] G. D. Paparo, M. Müller, F. Comellas, and M. A. Martin-Delgado, *Sci. Rep.* **3**, 2773 (2013).

[26] S. Boettcher and B. Gonçalves, *Europhysics Letters* **84**, 30002 (2008).

[27] D. A. Meyer, *Journal of Statistical Physics* **85**, 551 (1996).

[28] R. Portugal, S. Boettcher, and S. Falkner, (arXiv:1408.5166).

[29] A. N. Berker and S. Ostlund, *Journal of Physics C: Solid State Physics* **12**, 4961 (1979).

[30] M. Plischke and B. Bergersen, *Equilibrium Statistical Physics, 2nd edition* (World Scientific, Singapore, 1994).

[31] V. Singh and S. Boettcher, *Physical Review E* **90**, 012117 (2014).

[32] S. Redner, *A Guide to First-Passage Processes* (Cambridge University Press, Cambridge, 2001).

[33] S. Boettcher, S. Falkner, and R. Portugal, *Phys. Rev. A* **90** (2014).

[34] E. Domany, S. Alexander, D. Bensimon, and L. P. Kadanoff, *Phys. Rev. B* **28**, 3110 (1983).

## Appendix

While the methods presented for MK3 in the main text directly transfer to the other networks, we shall outline the procedure for them in more detail here.

First, we consider the case of MK4, which is similar to MK3 except that it features a different degree for each

site and, thus, establishes the conjecture for a different, rank  $r = 4$  Grover coin than for the other networks considered here, which all use the Grover coin of rank  $r = 3$ . We have focused on the lowest-rank coins because higher-ranked coins generally make the algebra more complex. However, this  $r = 4$  result demonstrates that the conjecture is likely robust on such a change.

MK4 follows the same idea as MK3 as every edge is replaced by multiple nodes and edges from one generation to the next. The smallest four-regular graph that can be consistently labeled with four different edge types such

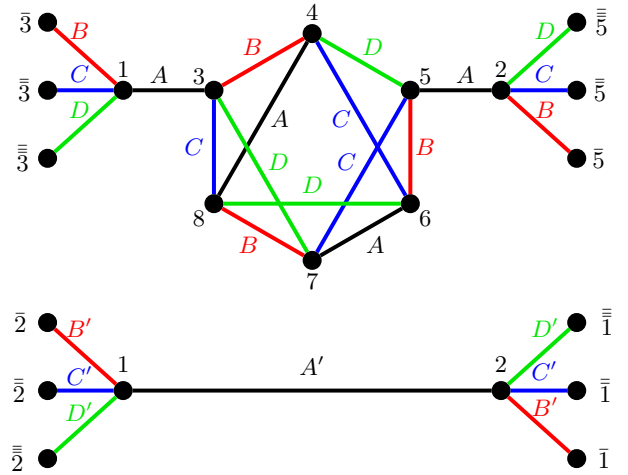


Figure 4. Iteration scheme for MK4. The six interior nodes  $3, \dots, 8$  and all their connections (top) are replaced by direct connection between 1 and 2 (bottom). The renormalized hopping parameter  $A'$  depends on all hopping matrices in the previous step. The construction of the network can be seen as the reverse process, inserting 6 nodes into every edge leaving the hopping parameter unchanged. The nodes labeled with overbars represent to analogous nodes where the same rule is applied. The scheme for  $B$ ,  $C$  and  $D$  is obtained by cyclic permutation of the shown graphlets.

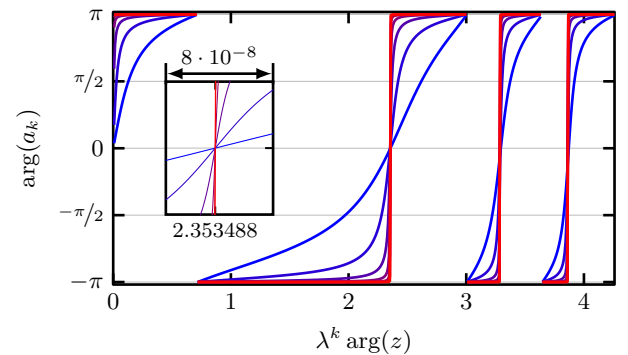


Figure 5. Scaling collapse of the phase of  $a_k$ , see Eqs. (17), near  $z = 1$ . The inset shows a magnification around the first intersection. In the main panel,  $k = 2, 6, \dots, 14$  while  $k = 20, 22, \dots, 30$  for the inset. This corresponds to a system sizes of  $N \approx 13^3 \approx 10^{34}$ . For the rescaling we used  $\lambda = \sqrt{247/7}$ .

that every node is connected to one of each kind contains 6 nodes, see Fig. 4. From the graphical representation, we can directly read off the linear system for the Laplace-transformed amplitudes on the interior nodes:

$$\begin{pmatrix} \tilde{\psi}_3 \\ \tilde{\psi}_4 \\ \tilde{\psi}_5 \\ \tilde{\psi}_6 \\ \tilde{\psi}_7 \\ \tilde{\psi}_8 \end{pmatrix} = \begin{bmatrix} A & 0 & M & B & 0 & 0 & D & C \\ 0 & 0 & B & M & D & C & 0 & A \\ 0 & A & 0 & D & M & B & C & 0 \\ 0 & 0 & 0 & C & B & M & A & D \\ 0 & 0 & D & 0 & C & A & M & B \\ 0 & 0 & C & A & 0 & D & B & M \end{bmatrix} \cdot \begin{pmatrix} \tilde{\psi}_1 \\ \tilde{\psi}_2 \\ \tilde{\psi}_3 \\ \tilde{\psi}_4 \\ \tilde{\psi}_5 \\ \tilde{\psi}_6 \\ \tilde{\psi}_7 \\ \tilde{\psi}_8 \end{pmatrix}. \quad (13)$$

Once the solution in terms of  $\tilde{\psi}_1$  and  $\tilde{\psi}_2$  is found, we can

plug it into the equations for, say,  $\tilde{\psi}_1$

$$\tilde{\psi}_1 = A\tilde{\psi}_3 + B\tilde{\psi}_4 + C\tilde{\psi}_5 + D\tilde{\psi}_6 \quad (14)$$

to find the renormalized system

$$\tilde{\psi}_1 = A'\tilde{\psi}_2 + B'\tilde{\psi}_1 + C'\tilde{\psi}_2 + D'\tilde{\psi}_1 \quad (15)$$

By studying the first few iterations, we choose the ansatz

$$\begin{aligned} A_k &= \frac{a+b}{2}(P_1 \cdot \mathcal{C}_G), & B_k &= \frac{a+b}{2}(P_2 \cdot \mathcal{C}_G), \\ C_k &= \frac{a+b}{2}(P_3 \cdot \mathcal{C}_G), & D_k &= \frac{a+b}{2}(P_4 \cdot \mathcal{C}_G), \\ M_k &= \frac{a-b}{2} \cdot (\mathbb{1} \cdot \mathcal{C}_G) \end{aligned} \quad (16)$$

capturing the evolution of all matrices. The  $P_\nu$  are the  $4 \times 4$  equivalent of the previously defined matrices, see Eqs. (16). Here the recursions for the parameters read

$$\begin{aligned} a_{k+1} &= \frac{-8a_k + 5a_k^3 + a_k^4 + (8+4a_k - 22a_k^2 - a_k^3 + 5a_k^4)b_k + (4+21a_k + 3a_k^2 - 30a_k^3 - 4a_k^4)b_k^2 + a_k(5+13a_k - 4a_k^2 - 16a_k^3)b_k^3}{-16 - 4a_k + 13a_k^2 + 5a_k^3 + (-4 - 30a_k + 3a_k^2 + 21a_k^3 + 4a_k^4)b_k + (5 - a_k - 22a_k^2 + 4a_k^3 + 8a_k^4)b_k^2 + (1 + 5a_k - 8a_k^3)b_k^3}, \\ b_{k+1} &= \frac{-8b_k + b_k^3 + a_k^3 b_k (5+4b_k - 16b_k^2) + a_k^2 (4+13b_k - 26b_k^2 - 12b_k^3) + a_k(8 - 12b_k - 18b_k^2 + b_k^3)}{-16 - 12a_k + a_k^2 + a_k^3 + 2(2 - 13a_k - 9a_k^2)b_k + (5 + 13a_k - 12a_k^2 - 8a_k^3)b_k^2 + 4a_k(1 + 2a_k)b_k^3}, \end{aligned} \quad (17)$$

where  $a_0 = b_0 = z$  as the initial conditions. These recursions resemble the ones in Eqs. (12), but the degrees of the polynomials in the numerator and denominator are higher. This is a direct consequence of the higher number of nodes eliminated during one iteration. Again, we have chosen a parametrization where  $|a_{k+1}| = |b_{k+1}| = 1$  if  $|a_k| = |b_k| = 1$ .

The rescaling of the phase of  $a_k$  is shown in Fig. 5. It is worth noting that for all networks considered here, all RG parameters scale equivalently. We just show one of them as an example, but we could use any one of them. The direct simulation for MK4 at  $k = 5$  ( $N = 2 \cdot 13^5 \approx 7 \cdot 10^5$ ) in Fig. 3 again confirms the RG prediction and the conjectured value of  $d_w^{QW}$ .

The derivation of RG recursions for HN3, see Fig. 6, is slightly more complicated than the above calculations for three reasons. First, the recursion on HN3 requires the introduction of a fourth hopping operator  $D$ , which is not present in the actual graph but becomes necessary to close the RG flow. Secondly, the symmetry of the hoppings is not preserved by the recursions. This means, after one decimation step, the matrix representing the hop from 1 to 2 is no longer identical with the one from 2 to 1. Lastly, the rules leading to HN3 inherently distinguish between even and odd sites. As a result, the self-interaction terms become different for those two groups. Therefore we have to introduce  $M_1$  on even and

$M_2$  on odd indices. If we make the ansatz

$$\begin{aligned} A &= \begin{bmatrix} \frac{b-a}{4} & \frac{a+b+2c}{4} & 0 \\ 0 & 0 & 0 \\ 0 & 0 & 0 \end{bmatrix} \cdot \mathcal{C}_G, & C &= P_3 \cdot \mathcal{C}_G, \\ B &= \begin{bmatrix} 0 & 0 & 0 \\ \frac{a+b+2c}{4} & \frac{b-a}{4} & 0 \\ 0 & 0 & 0 \end{bmatrix} \cdot \mathcal{C}_G, & D &= \begin{bmatrix} 0 & \frac{b-a}{4} & 0 \\ 0 & 0 & 0 \\ 0 & 0 & 0 \end{bmatrix} \cdot \mathcal{C}_G, \\ M_1 &= \frac{a+b-2c}{4}(P_1 + P_2) \cdot \mathcal{C}_G, & M_2 &= M_1 + D + D^T \end{aligned} \quad (18)$$

we can take everything into account by writing the linear system corresponding to the top right graphlet in Fig. 6 as

$$\begin{aligned} \tilde{\psi}_4 &= A^T \tilde{\psi}_1 + B^T \tilde{\psi}_2 + M_2 \tilde{\psi}_4 + C \tilde{\psi}_5 \\ \tilde{\psi}_5 &= A^T \tilde{\psi}_2 + B^T \tilde{\psi}_3 + C^T \tilde{\psi}_4 + M_2 \tilde{\psi}_5 \end{aligned} \quad (19)$$

Here  $A^T$  represents the transpose of  $A$ , which, incidentally, correctly describes the hopping in opposite directions (left-to-right for  $A$  and right-to-left for  $A^T$  in the figure).

By solving these equations for  $\tilde{\psi}_4$  and  $\tilde{\psi}_5$ , and inserting this into the equations for the remaining sites,

$$\begin{aligned} \tilde{\psi}_1 &= M_1 \tilde{\psi}_1 + D \tilde{\psi}_2 + D^T \tilde{\psi}_1 + A \tilde{\psi}_4 + B^T \tilde{\psi}_5 + C \tilde{\psi}_* \\ \tilde{\psi}_2 &= D \tilde{\psi}_1 + M_1 \tilde{\psi}_2 + D^T \tilde{\psi}_3 + B^T \tilde{\psi}_4 + A \tilde{\psi}_5 + C \tilde{\psi}_*, \end{aligned} \quad (20)$$

we find the recursion equations for the three RG variables by identifying the terms corresponding in

$$\begin{aligned}\tilde{\psi}_1 &= M'_1 \tilde{\psi}_1 + A' \tilde{\psi}_2 + B'^T \tilde{\psi}_2 + D' \tilde{\psi}_3 + D'^T \tilde{\psi}_3 + C \tilde{\psi}_*, \\ \tilde{\psi}_2 &= A'^T \tilde{\psi}_1 + M_2 \tilde{\psi}_2 + B \tilde{\psi}_3 + C \tilde{\psi}_*.\end{aligned}\quad (21)$$

Note that the equation for  $\tilde{\psi}_3$  is up to a simple relabeling of the indices equivalent to the first one, and every site is connected to a site of unknown index,  $\tilde{\psi}_*$ , but the corresponding hopping matrix  $C$  does not change. After some algebra, we find

$$\begin{aligned}a_{k+1} &= \frac{c_k(-3+z) - b_k(-3+z + c_k(-2+6z))}{6 - b_k + c_k + (-2+3b_k - 3c_k)z}, \\ b_{k+1} &= \frac{c_k(3+z) - b_k(3+z + c_k(2+6z))}{-6 + b_k - c_k + (-2+3b_k - 3c_k)z}, \\ c_{k+1} &= \frac{c_k + a_k(-1+2c_k)}{2 + a_k - c_k},\end{aligned}\quad (22)$$

with the initial conditions

$$a_0 = \frac{z^2(1-3z)}{3-z}, \quad b_0 = \frac{z^2(1+3z)}{3+z}, \quad c_0 = z^2. \quad (23)$$

Again, we have chosen our ansatz such that the variables stay of modulus one when they start out that way.

This time we show the rescaling of the argument of the first RG parameter in Fig. 7. As further justification, we also scale the numerically obtained PDF for HN3 in Fig. 3.

Finally, we consider the DSG, see Fig. 8. In order to make it renormalizable, we have to introduce a directionality represented by the arrows for  $A$  and  $B$ . This just

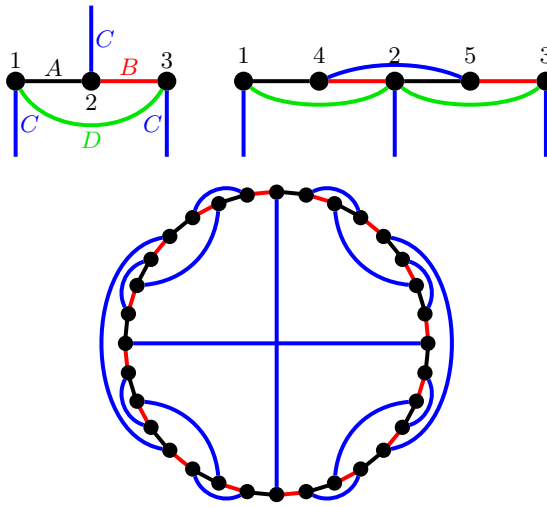


Figure 6. Illustration of the decimation scheme for HN3. Growing the network means inserting new sites (4 and 5) and connecting them accordingly (top row). The graph at generation  $k = 5$  is shown in the lower panel. The RG decimation requires an extra set of hopping operators ( $D$ , green) not present in the actual network in order to close the recursions.

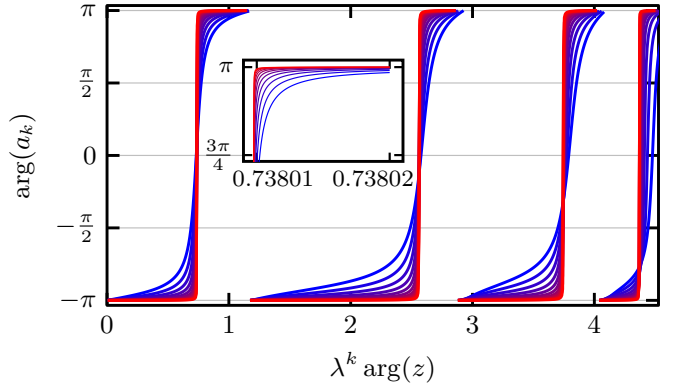


Figure 7. (color online) Rescaling of the phase of the first RG parameter  $a_k$  around the fixed point  $z = 1$ . The insets show a magnification to illustrate the conversion towards a step function. In the main panel,  $k = 10, 12, \dots, 30$  while  $k = 60, 62, \dots, 80$  for the inset. This means the largest system size is  $N \approx 10^{24}$ . For the rescaling, we used  $\lambda = \sqrt{24 - 8\sqrt{5}}$ .

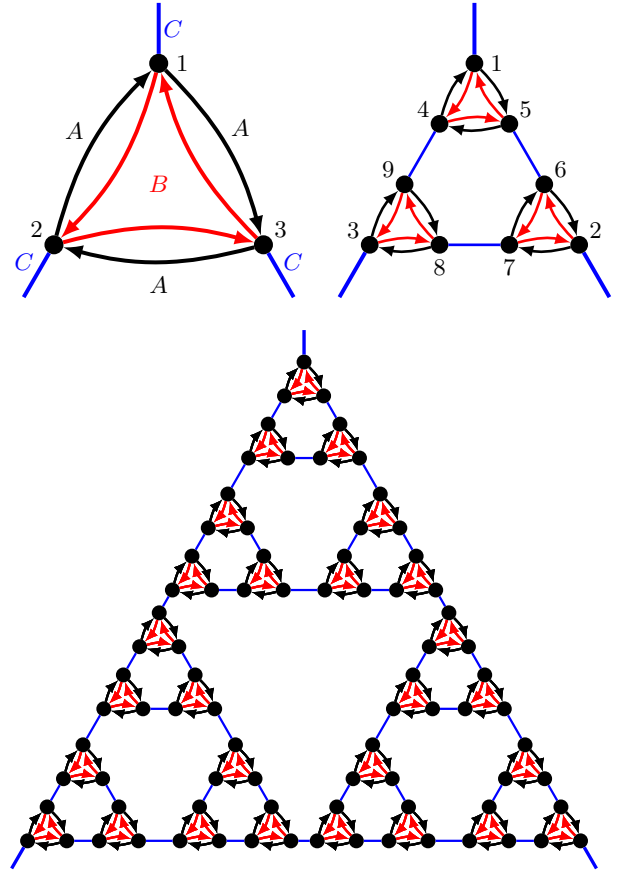


Figure 8. The well known recursion generating the DSG (top row). To make the positions of the hopping matrices also self-similar, we have to introduce directionality of the hopping matrices  $A$  and  $B$ . The third one,  $C$ , is still symmetric. The lower panel shows the system at generation four.

means that applying one hopping matrix, say  $A$ , twice describes the hopping from site 1 to 2 (over 3), and not 1 to 3 back to 1. The matrix  $C$  is not affected by this.

The linear system we need to solve in this case reads

$$\begin{pmatrix} \tilde{\psi}_4 \\ \tilde{\psi}_5 \\ \tilde{\psi}_6 \\ \tilde{\psi}_7 \\ \tilde{\psi}_8 \\ \tilde{\psi}_9 \end{pmatrix} = \begin{bmatrix} B & 0 & 0 & M & A & 0 & 0 & 0 & C \\ A & 0 & 0 & B & M & C & 0 & 0 & 0 \\ 0 & B & 0 & 0 & C & M & A & 0 & C \\ 0 & A & 0 & 0 & 0 & B & M & C & 0 \\ 0 & 0 & B & 0 & 0 & 0 & C & M & A \\ 0 & 0 & A & C & 0 & 0 & 0 & B & M \end{bmatrix} \begin{pmatrix} \tilde{\psi}_1 \\ \tilde{\psi}_2 \\ \tilde{\psi}_3 \\ \tilde{\psi}_4 \\ \tilde{\psi}_5 \\ \tilde{\psi}_6 \\ \tilde{\psi}_7 \\ \tilde{\psi}_8 \\ \tilde{\psi}_9 \end{pmatrix} \quad (24)$$

The results then has to be plugged into the equations for  $\tilde{\psi}_1, \dots, \tilde{\psi}_3$ :

$$\begin{aligned} \tilde{\psi}_1 &= A\tilde{\psi}_4 + B\tilde{\psi}_5 + C\tilde{\psi}_{\bar{2}/\bar{3}} \\ \tilde{\psi}_2 &= A\tilde{\psi}_6 + B\tilde{\psi}_7 + C\tilde{\psi}_{\bar{1}} \\ \tilde{\psi}_3 &= A\tilde{\psi}_8 + B\tilde{\psi}_9 + C\tilde{\psi}_{\bar{1}} \end{aligned} \quad (25)$$

Here the algebra is very involved, and we have shown [33] how it can be done. In the same reference, we showed the scaling of the parameters and deduced  $d_w^{QW}$  from it using the RG. The scaling collapse for DSG in Fig. 3 confirms again the conjecture.